

A THEORY OF SOLAR TYPE IV EMISSION ON CENTIMETRE AND DECIMETRE WAVELENGTHS

By W. K. YIP*

[Manuscript received May 14, 1967]

Summary

Assuming models for electron density and magnetic field configuration in the lower solar active corona, it is proposed that type IV bursts on centimetre and decimetre wavelengths are the results of cyclotron radiation from helical electron streams. In order to explain the observed polarization features and spectral variabilities, the characteristics of cyclotron radiation from electron streams and the propagation of electromagnetic waves in the active corona are investigated. Adopting the current model for flare evolution, most of the properties of type IV bursts on centimetre and decimetre wavelengths are well interpreted by the present theory.

I. INTRODUCTION

Immediately after the occurrence of large flares, long periods of enhanced continuum radiation superimposed with fast-drift bursts may be observed. Such emission occurs in a frequency range from a few hundred to several thousand megahertz and lasts for a period of a few tens of minutes or hours. Usually, it is associated with the type IV bursts on metre wavelength (designated as type IVm), which possess similar spectral characteristics. Therefore this enhanced continuum emission superimposed with variabilities on centimetre and decimetre wavelengths is regarded as the first phase of the whole type IV emission, and is designated as type IVA by Kundu (1965), or type IV μ (microwave type IV) by Wild, Smerd, and Weiss (1963), or type IV group A and group A-B by Takakura and Kai (1961), while type IVm bursts are regarded as second and third phase emissions. (In the present paper, Kundu's nomenclature is used.) Dynamic spectrum and single-frequency observations in various frequency ranges have been reported by Haddock (1959), Takakura (1960*a*, 1963), Kundu (1961), Pick (1961), Young *et al.* (1961), and Thompson and Maxwell (1962). From all the observational records, the spectral features and the source characteristics of type IVA emission can be summarized as follows.

(i) Frequency Range

Type IVA continuum occurs from frequencies higher than 10 000 MHz and extends down to 200 MHz. The frequencies of the fast-drift elements that are superimposed on the background continuum mostly lie within the range 300–1000 MHz (decimetre wavelength region) (Kundu 1965).

(ii) Intensity

The intensity varies from a barely detectable value of about 5×10^{-22} W m⁻² Hz⁻¹ to greater than 10^{-18} W m⁻² Hz⁻¹. For great bursts (associated with

* Physics Department, University of Tasmania, Hobart.

type IVm bursts) the decimetre wavelength burst intensity is usually less than that of the centimetre or metre wavelength bursts. The intensity of the fast-drift bursts is higher and can reach $10^{-18} \text{ W m}^{-2} \text{ Hz}^{-1}$. There is some tendency for the intensity to decrease with the frequency (Kundu 1965).

(iii) *Bandwidth*

The continuum in centimetre and decimetre wavelength regions extends over hundreds of megahertz. Dynamic spectra (Kundu *et al.* 1961; Thompson and Maxwell 1962) indicate that type IVA emission consists of groups of very broad band bursts, which occur in rapid sequence and which may be superimposed upon each other or may merge together to form a continuum. The bandwidth of decimetre wavelength emission is narrower than that of centimetre wavelength emission. The drifting elements in the decimetre wavelength region have bandwidths as narrow as 10 MHz.

(iv) *Variabilities*

The dynamic spectra of the long duration centimetre wavelength bursts show a broad band smooth continuum and lack complexity, while in the decimetre wavelength region the smooth continuum has very short duration drift bursts superimposed on it.

(v) *Frequency Drift*

Only a few decimetre wavelength continuum bursts show a steady and slow drift from high frequencies towards lower frequencies. The drift rate is roughly estimated to be 200 MHz/hr (Takakura 1963). The drift bursts on the other hand may have a frequency drift greater than 2000 MHz/sec. Both senses of drift are observed (Young *et al.* 1961; Kundu and Spencer 1963).

(vi) *Duration*

Thompson and Maxwell (1962) reported that typical durations of the event are 5–40 min in the centimetre wavelength region and 5–120 min in the decimetre wavelength region. Individual fast-drift bursts have durations of the order of half a second.

(vii) *Polarization*

The centimetre and decimetre wavelength continuum bursts are partially circularly polarized and the sense of polarization may change between 2000 and 4000 MHz. If the leading sunspot is taken to have north polarity, then at high frequencies the polarization is in the extraordinary mode but changes to the ordinary mode at decimetre wavelengths. The degree of polarization increases towards lower frequencies (Takakura 1963; Kundu 1965).

(viii) *Position and Movement of the Sources*

At all frequencies ranging from 9400 to 340 MHz the source is situated less than 40 000 km above the photosphere. Significant movement of the type IVA source has not been observed (Kundu 1959; Kundu and Firor 1961).

(ix) *Association with Flares*

The type IVA burst emissions are strongly associated with solar flares. The percentage of solar flares that are associated with type IV bursts on centimetre wavelength increases with flare importance (reaching nearly 100% for flares of importance 3). The association of flares with decimetre wavelength bursts is not so strong (for flares of importance 2 and 3 the association is about 25 and 85% on 545 MHz, as compared with about 40 and 100% on 3000 MHz). A flare has a greater probability of being associated with a type IV burst if the flare area covers the umbra of the active region where the flare originates. The time of start of type IVA bursts appears to coincide with the explosive phase rather than with the commencement of the associated flares. In nearly all observable cases there are groups of type III bursts almost in coincidence with the explosive phase of the flare. Sometimes, for a flare of great importance, the type III bursts are followed by type II and type IVm bursts. The flares associated with type IV without type II bursts are of less importance than those associated with type IV-type II bursts (Kundu 1965).

(x) *Association with Metre Wavelength Bursts*

Type IVA bursts can occur with or without type II bursts on metre wavelengths. In the frequency range 250–580 MHz type IV emission (decimetre wavelength) in most cases occurs a few minutes earlier than the associated type II bursts, but, on frequencies less than 250 MHz, type IV emission (metre wavelength) follows the occurrence of type II. The centimetre wavelength bursts associated with type IV-type II events have stronger intensity and the importance of the associated flares is also greater (Kundu 1965).

(xi) *Directivity and Angular Size*

Type IVA bursts on centimetre wavelength do not exhibit any directivity, but on decimetre wavelength they show slight directivity towards the centre of the Sun (Takakura 1963). The diameter of the source is 2–4 min of arc (Wild, Smerd, and Weiss 1963), which is less than that of a type I noise storm.

Type IV emission on metre wavelength was first discovered by Boischoot (1957) and was interpreted as a consequence of incoherent synchrotron radiation from electrons of energy of a few million electron-volts gyrating in the sunspot magnetic field (Boischoot and Denisse 1957). Takakura (1960b, 1960c) and Takakura and Kai (1961) used the synchrotron radiation theory to explain the whole type IV event in different phases and on different wavelengths. In order to explain the reverse of sense of polarization, without taking account of differential harmonic resonance absorption, Takakura (1962) suggested that the centimetre wavelength type IV was associated with synchrotron radiation from electrons of energy of the order of a few hundred keV accumulated above the leading spot while the decimetre wavelength type IV source was above the following spot. The type IVA bursts on centimetre and decimetre wavelengths have separate sources. Kundu (1965) pointed out that the narrow bandwidth of decimetre wavelength bursts cannot be explained as synchrotron radiation; radiation from plasma waves may be a possible mechanism. The drift

bursts that are superimposed on the smooth continuum are considered as plasma radiation induced by passage of a disturbance travelling outward through the solar corona with speed $\sim \frac{1}{2}c$ (Young *et al.* 1961).

Since the type IVm bursts possess spectral characteristics similar to the type IVA bursts, the above theories have also been used to explain type IVm burst emission (Denisse 1960; Takakura and Kai 1961). However, interpreting the type IVm and type IVA emissions as synchrotron radiation and plasma radiation meets various difficulties. The reasons are given by Fung (1967). Any theory of type IVA emission has to explain, in particular, the change of polarization with frequency and the variabilities that are superimposed on the decimetre wavelength continuum. Recently Fung and Yip (1966) after studying the propagation conditions of electromagnetic waves in the solar corona found that the type I noise storm superimposed with narrow-band bursts can be well accounted for by Doppler-shifted cyclotron radiation from electron streams gyrating in magnetic field configurations of sunspots. Therefore, it seems possible that the same mechanism may be responsible for type IVA burst emissions on centimetre and decimetre wavelengths. It is the purpose of the present paper, by adopting the generally accepted model for the evolution of flare phenomena (Kundu 1965), to examine the possibility that the cyclotron radiation process is the origin of type IVA burst emissions.

II. MODEL OF THE SOLAR CORONA

We begin by assuming a model for the solar atmosphere in the active coronal region so that the theory can be discussed quantitatively. The generally accepted radial electron density distribution in the quiet corona is given by the Baumbach–Allen formula (Allen 1947)

$$N = 10^8(1.55\rho^{-6} + 2.99\rho^{-16}), \quad (1)$$

where N is the number of electrons per cubic centimetre, $\rho = R/R_0$, R is the radial distance from the centre of the Sun, and R_0 is the radius of the photosphere (6.95×10^5 km). Optical and radio observations indicate that the electron density in the active coronal region above the sunspot group increases from several to 10 times that given by (1) (Newkirk 1959; Shain and Higgins 1959; Morimoto and Kai 1961; Weiss 1963). The formula (1) is applied to the coronal region at a height greater than 10^4 km above the photosphere. In the chromosphere, the electron density and electron density gradient are very high. Recently Ivanov-Kholodnyi and Nikol'skii (1962), from a detailed analysis of observational data, obtained the distribution of electron density with height in active and undisturbed regions of the solar atmosphere. Using their result, the plasma frequency along the active corona from $\rho = 1.005$ to 1.043 is plotted in Figure 1. The curve is smoothly continued by employing the $5 \times$ Baumbach–Allen formula.

About 90% of all sunspot groups are of bipolar character; the magnetic field lines coming from the leading spot and from the following spot form complete loops. During the solar active period the magnetic field intensity at the centre of the sunspot is found to be of the order of 2000–4000 G. A bipolar field is of dipole nature and its variation of intensity with height, as described in Fung and Yip (1966),

can be found by assuming that an image dipole is buried just beneath the photosphere and that field lines coming from the dipole pass through the area of the sunspot. Taking the maximum field intensity of the leading spot to be $H_s = 3000$ G, we set up the model for the sunspot magnetic field intensity as shown in Figure 1. If the type IVA emissions whose frequencies range from 500 to 10 000 MHz are the result of cyclotron radiation from electron streams gyrating along sunspot magnetic field lines, the region of emission will be less than 40 000 km above the photosphere.

It is convenient to describe the active coronal medium by a single quantity A , which is defined as $A = f_p^2/f_H^2$, where $f_p = (e^2N/\pi m_0)^{1/2}$ is the electron plasma frequency and $f_H = eH/m_0c$ is the electron gyrofrequency. From Figure 1, within the type IVA emission source region A is seen to vary from a very small value to about 1.5.

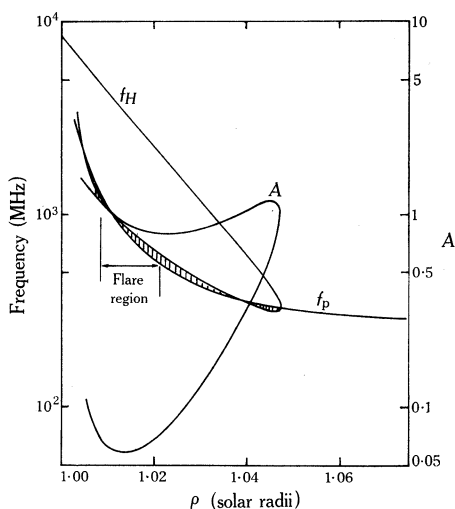


Fig. 1.—Variation of plasma frequency f_p (using the Ivanov-Kholodnyi and Nikol'skii model and the $5 \times$ Baumbach-Allen model), gyrofrequency f_H , and A along a bipolar spot pair specified by $H_s = 3000$ G.

III. RADIATION FROM ELECTRON STREAMS IN SUNSPOT MAGNETIC FIELD CONFIGURATIONS

During the occurrence of a very large flare, electrons with energy 10–100 keV (occasionally more) in the form of electron streams are expelled from the flare region (De Jager 1960). Most of these electron streams will be trapped in the neighbouring strong sunspot magnetic field and will interact with the ambient plasma. Harmonic cyclotron radiation in the ordinary and extraordinary modes from the stream electrons will grow as they propagate through the stream-plasma system (Fung 1966a). Using the model indicated in Section II for the type IVA emission source medium, we shall study the characteristics of forward normal cyclotron radiation from streams of electrons with energy 100 keV for different electron pitch angles ϕ . The backward normal radiation has been studied by Fung (1967) and it is found that in general the backward radiation power is smaller than the forward power. In the following discussion of this section, we assume that the coronal magnetoactive plasma is cold and collisionless. This assumption, in most cases, is valid (Fung and Yip 1966).

(a) Radiation Frequency

A single electron spiralling along a magnetic field line of force radiates electromagnetic waves of different frequencies and of different modes (ordinary and extraordinary) in different directions. The relation between the normalized radiation frequency ξ , defined as the ratio of the radiation frequency to the gyro-frequency, and the wave-normal angle θ is given by the emission equation (Liemohn 1965)

$$\xi = s\gamma/(1 - n_j \beta_{\parallel} \cos \theta), \tag{2}$$

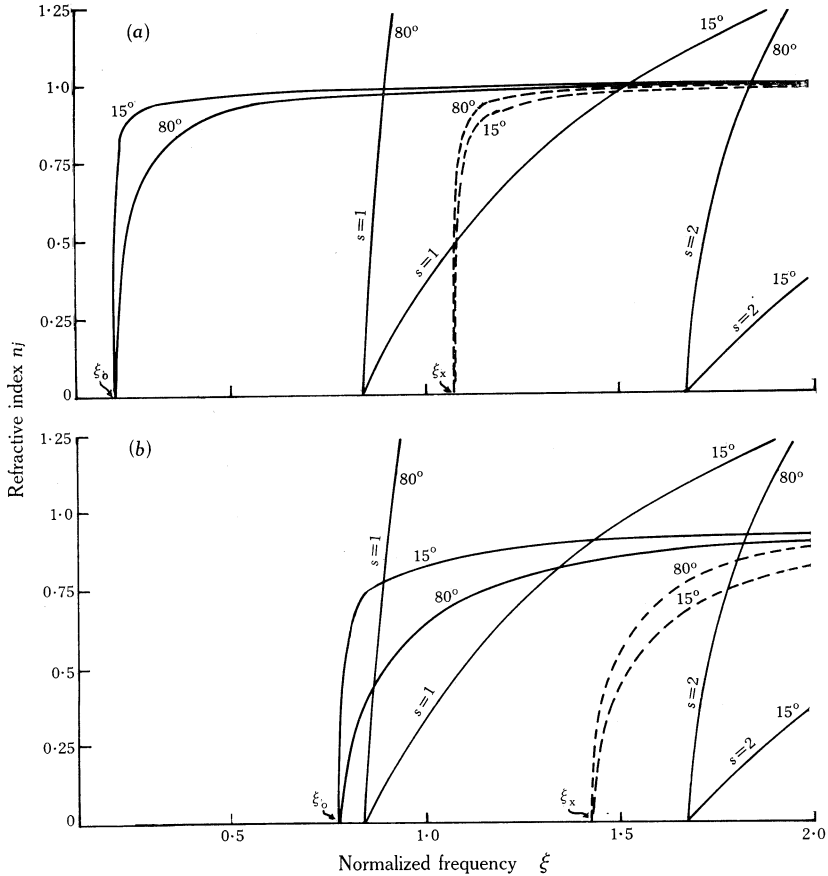


Fig. 2.—Refractive index n_j for the o-mode (full lines) and x-mode (dashed lines) against the normalized wave frequency ξ for (a) $A = 0.04$, (b) $A = 0.6$, and $\theta = 15^\circ$ and 80° . The emission equation is also plotted for the first two harmonics $s = 1, 2$ as a function of ξ for electron energy $E = 100$ keV and electron pitch angle $\phi = 30^\circ$.

where $\beta_{\parallel} = v_{\parallel}/c$, $\beta_{\perp} = v_{\perp}/c$, with v_{\parallel} and v_{\perp} the electron velocity components parallel and perpendicular to the magnetic field respectively, $\gamma = (1 - \beta^2)^{-1/2}$ is the relativistic correction factor, with $\beta^2 = \beta_{\parallel}^2 + \beta_{\perp}^2$, s is the harmonic number, and n_j is the refractive index for the ordinary wave ($j = 2$) or the extraordinary wave ($j = 1$) in the

ambient plasma. For a cold and collisionless plasma

$$n_j^2 = 1 - A \left\{ \xi^2 - \frac{\xi^2 \sin^2 \theta}{2(\xi^2 - A)} \mp \left(\frac{\xi^4 \sin^4 \theta}{4(\xi^2 - A)^2} + \xi^2 \cos^2 \theta \right)^{\frac{1}{2}} \right\}^{-1}. \quad (3)$$

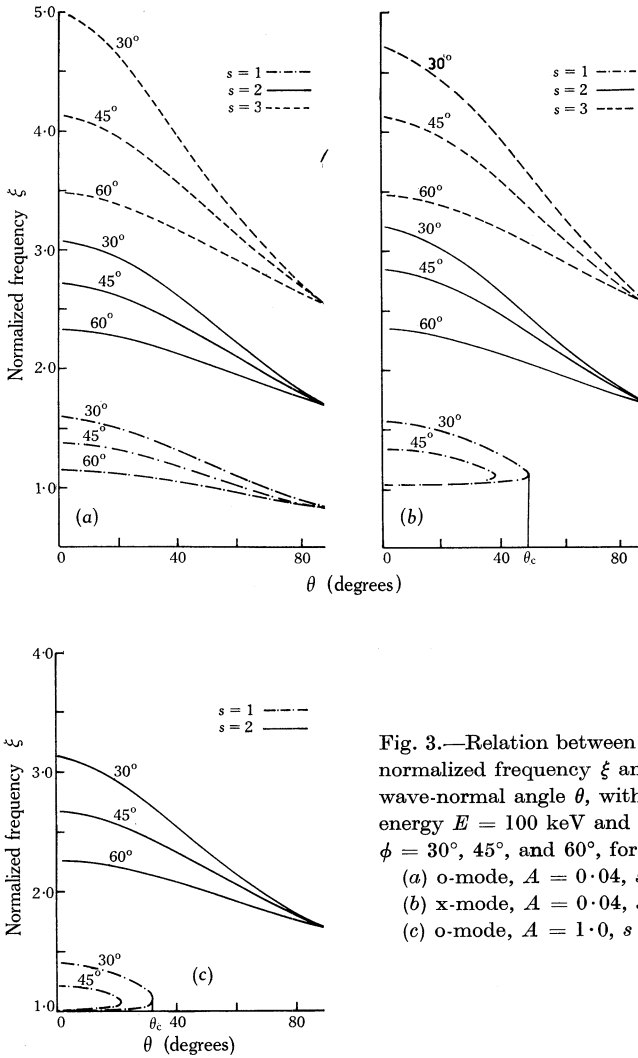


Fig. 3.—Relation between normalized frequency ξ and wave-normal angle θ , with electron energy $E = 100$ keV and pitch angle $\phi = 30^\circ, 45^\circ,$ and 60° , for
 (a) o-mode, $A = 0.04, s = 1, 2, 3$;
 (b) x-mode, $A = 0.04, s = 1, 2, 3$;
 (c) o-mode, $A = 1.0, s = 1, 2$.

In order to find the normalized radiation frequency in a particular direction with respect to the magnetic field, equations (2) and (3) must be solved simultaneously by algebraic or graphical methods (Ellis 1964). The curves of refractive index n_j against normalized frequency ξ for various values of θ and $s > 0$ (normal radiation) from (2) and (3) are plotted in Figure 2. Figure 3 shows the simultaneous solutions for ξ and θ of (2) and (3).

It has been shown by Fung and Yip (1966) that there are two types of simultaneous solutions for ξ and θ :

- (1) the double-frequency solution, i.e. to each wave-normal angle there correspond two normalized frequencies;
- (2) the single-frequency solution, i.e. only one normalized frequency corresponds to one wave-normal angle.

The double-frequency solution is possible when

$$\text{or } \left. \begin{aligned} s\gamma < \xi_o &= A^{\frac{1}{2}} && \text{(o-mode)} \\ s\gamma < \xi_x &= \frac{1}{2}\{1+(1+4A)^{\frac{1}{2}}\} && \text{(x-mode).} \end{aligned} \right\} \quad (4)$$

Whenever conditions (4) are satisfied, the radiation is emitted within a cone with apex angle $2\theta_c$ and the direction of the magnetic field as axis. The angle θ_c is the angle beyond which there is no radiation at all and is termed the cutoff angle. For conditions other than (4) we have a single-frequency solution only. We note that in certain cases, e.g. for a very large electron pitch angle or ξ_o (or ξ_x) $\gg s\gamma$, there is no simultaneous solution of any type for ξ and θ . For both o-mode and x-mode, the range of the radiation frequency is wider for smaller electron pitch angles.

(b) Power Spectra radiated by a Single Electron

Corresponding to the values of normalized frequency ξ and wave-normal angle θ obtained by solving equations (2) and (3) simultaneously, the radiation power by a single electron within unit solid angle can be computed by using the equation (Liemohn 1965)

$$P(\theta) = \left(\frac{e^2}{2\pi c} \right) \left(\frac{\omega^2 n_j K^2 \{ -\beta_{\perp} J'_s(a) + (\alpha_y s \beta_{\perp}/a + \alpha_z \beta_{\parallel}) J_s(a) \}^2 \{ 1 + (\omega/n_j) \partial n_j / \partial \omega \}}{|1 - \beta_{\parallel} n_j \cos \theta \{ 1 + (\omega/n_j) \partial n_j / \partial \omega \}|} \right), \quad (5)$$

where

$$\alpha_y = \alpha_{\theta} \cos \theta + \alpha_K \sin \theta, \quad \alpha_z = \alpha_K \cos \theta - \alpha_{\theta} \sin \theta,$$

$$K = (1 + \alpha_{\theta}^2)^{-\frac{1}{2}},$$

$$\alpha_{\theta} = -\xi \cos \theta / \{ \xi^2 + A(n_j^2 - 1)^{-1} \}, \quad \alpha_K = -\xi \sin \theta (n_j^2 - 1) / (A - \xi^2),$$

J_s and J'_s are the Bessel function and its derivative with argument $a = \beta_{\perp} \xi \sin \theta n_j / \gamma$, and n_j is the refractive index given by (3). For electron energy $E = 100$ keV, $A = 0.04$ and 1.0 , $s = 1, 2$, and 3 , and electron pitch angle $\phi = 60^\circ, 45^\circ$, and 30° , the power spectra radiated by a single electron in o-mode and x-mode are presented in Figure 4. From these spectra, the following points are noted:

- (1) For the double-frequency solution, the radiation power peaks sharply at wave-normal angles near θ_c .
- (2) For the single-frequency solution and $s = 2$ and 3 , the o-mode power reaches a maximum in wave-normal angles ranging from 50° to 70° , while for the x-mode the emission cone is very broad.
- (3) For the single-frequency solution, radiation power for both the o-mode and the x-mode is inversely proportional to the harmonic number.

- (4) For the same set of values of A , s , ϕ , and E , the peak power radiated by a single electron is about one order of magnitude higher in the x-mode than in the o-mode.

(c) *Excitation of Cyclotron Radiation in the Stream-Plasma System*

At present it is known that electromagnetic waves emitted from gyrating electrons can be amplified in a stream-plasma system if the distribution of stream electrons has a narrow momentum spread. Using the classical kinetic approach, the radiative instability problem of a helical electron stream-plasma system has

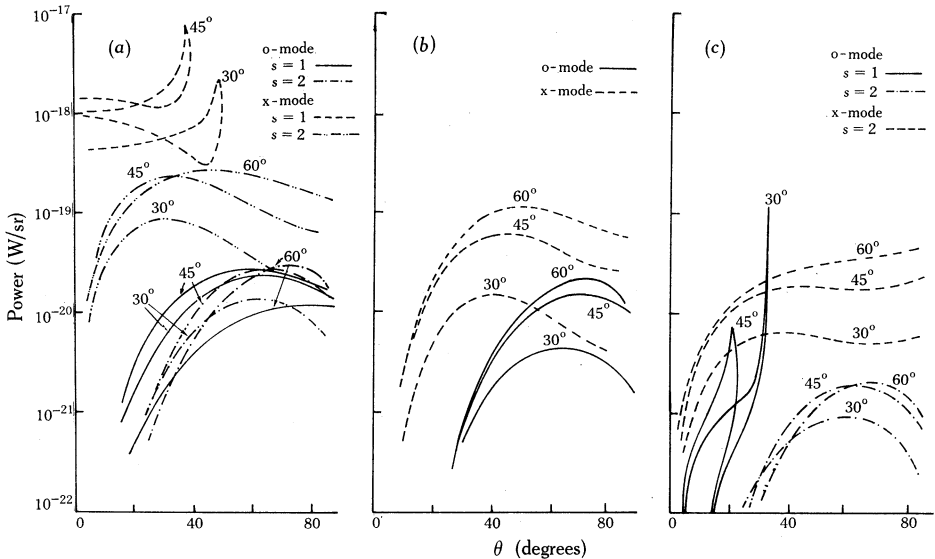


Fig. 4.—Power spectra radiated by a single electron, with energy $E = 100$ keV and electron pitch angle $\phi = 30^\circ, 45^\circ,$ and 60° , for o-mode and x-mode, various values of s , and

(a) $A = 0.04, f_H = 1000$ MHz;

(b) $A = 0.04, f_H = 1000$ MHz, $s = 3$ for both modes;

(c) $A = 1.0, f_H = 300$ MHz.

been solved for the most general cases and applied to the interpretation of radio emissions from the Sun, the exosphere, and Jupiter (Fung 1966a, 1966b, 1967; Fung and Yip 1966). Assuming no dispersion of the electrons in the momenta p_\perp and p_\parallel , the undisturbed distribution function of the electrons in a helical stream has the form

$$f_0(\vec{p}) d\vec{p} = (1/2\pi p_\perp^0) \delta(p_\perp - p_\perp^0) \delta(p_\parallel - p_\parallel^0) d\vec{p}, \quad (6)$$

where p_\perp, p_\parallel are transverse and longitudinal momenta with respect to the magnetic field direction respectively, p_\perp^0 and p_\parallel^0 are corresponding values where the distribution curve reaches the maximum, and δ is the Dirac delta. With this distribution for stream electrons, the rate of growth of an electromagnetic wave in the stream-plasma system $|\text{Im } \delta|$ is given by

$$\text{Im}(\delta/\bar{\omega}) = \pm(\frac{1}{2}\sqrt{3})(M^\ddagger - C^\ddagger), \quad (7)$$

where

$$M = -\frac{1}{2}d + (\frac{1}{4}d^2 + b^3/27)^{\frac{1}{3}} \quad \text{and} \quad C = -\frac{1}{2}d - (\frac{1}{4}d^2 + b^3/27)^{\frac{1}{3}},$$

$$\text{with} \quad b = -\sigma A J_s^2 \left(\frac{(s\gamma - \xi)^2}{\beta_{\parallel}^2 \xi^2} - 1 \right) \frac{\beta_{\parallel}^2 \cos^2 \theta}{(\xi - s\gamma)^2},$$

$$d = \sigma A \left(\frac{(s\gamma - \xi)^2}{\beta_{\parallel}^2 \xi^2} - 1 \right) \frac{J_s'^2 \beta_{\perp}^2 + J_s^2 \beta_{\parallel}^2 (s\gamma - \xi \sin^2 \theta)^2 / (s\gamma - \xi)^2 \sin^2 \theta}{(AL - 2\xi^2)},$$

$$\sigma = \omega_0^2 / \omega_p^2 = (\text{density of stream}) / (\text{density of ambient plasma}),$$

$$L = \frac{1}{D^2} \left[\frac{2AD}{\xi^2} - \left(1 - \frac{A}{\xi^2} \right) \left\{ \frac{2A}{\xi^2} + \frac{\sin^2 \theta}{\xi^2} - B^{-\frac{1}{2}} \left[\frac{-\sin^4 \theta}{\xi^4} + \frac{4A \cos^2 \theta}{\xi^4} \left(1 - \frac{A}{\xi^2} \right) - \frac{2 \cos^2 \theta}{\xi^2} \left(1 - \frac{A}{\xi^2} \right)^2 \right] \right\} \right],$$

$$D = 1 - A\xi^{-2} - \frac{1}{2}\xi^{-2} \sin^2 \theta - B^{\frac{1}{2}},$$

$$\text{and} \quad B = \frac{1}{4}\xi^{-4} \sin^4 \theta + \xi^{-2} \cos^2 \theta (1 - A\xi^{-2})^2.$$

$\tilde{\omega}$ is the angular wave frequency. Again the normalized frequency ξ and wave-normal angle θ must satisfy the emission equation (2). Taking $\sigma = 10^{-4}$ and various values of the other parameters, the rates of growth of cyclotron radiation power are illustrated in Figure 5. These graphs indicate:

- (1) With the same values of f_H , s , and σ , both x-mode and o-mode powers grow at a similar rate with time when A is small, but as A increases the growth rate for o-mode power exceeds that for x-mode power.
- (2) For the single-frequency solution and for both x-mode and o-mode, the growth rate maximizes for wave-normal angle $\theta \sim 50^\circ - 70^\circ$.
- (3) In the cases of a single-frequency solution for the x-mode and o-mode, when ϕ , E , A , and f_H are fixed the growth rate for third harmonic radiation is smaller than that for second harmonic radiation; the first and second harmonic radiations grow at a similar rate with time.
- (4) If t is the interaction time, the power gain factor is $\exp(2|\text{Im} \delta|t)$. After growth in the stream-plasma system for 10^{-6} sec, the second harmonic x-mode and o-mode power spectra radiated by a single electron are shown in Figure 6. It can be seen that after growth the powers of both modes peak at a similar wave-normal angle $\theta \sim 65^\circ$ and the ratio of x-mode power to o-mode power (denoted by r) does not exceed 10. The normalized frequency corresponding to the peak emission power is $\xi \gtrsim s$ when the electron pitch angle is not too large ($< 45^\circ$).
- (5) Because of (1), the ratio r decreases with increasing values of A .
- (6) For the single-frequency solution in either mode, the half-power emission cone (hence the bandwidth) is broad if the interaction time is not large, whereas for the double-frequency solution the emission cone is narrow.

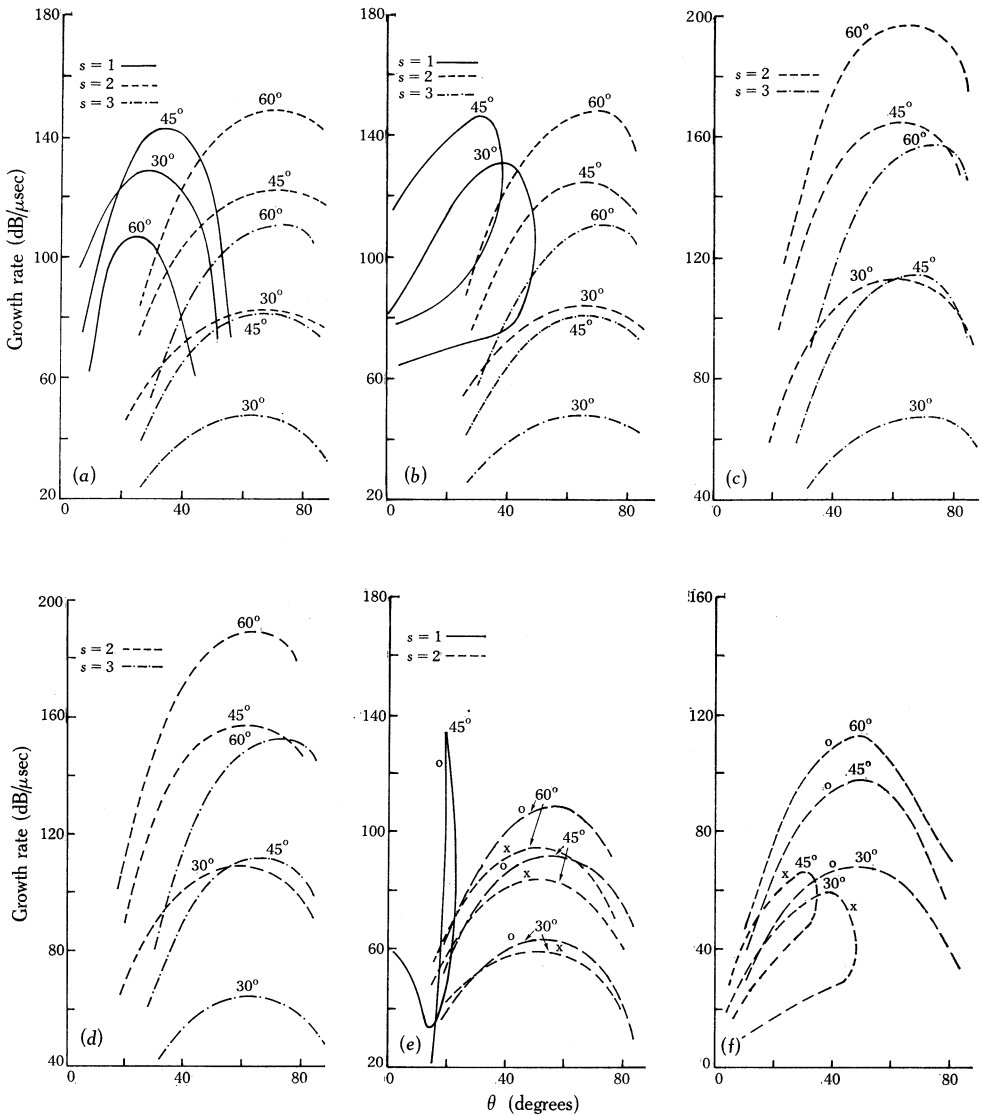


Fig. 5.—The dependence of the growth rate $|\text{Im } \delta|$ on wave-normal angle θ , with $\sigma = 10^{-4}$, $E = 100$ keV, and $\phi = 30^\circ, 45^\circ$, and 60° , for

- (a) o-mode, $A = 0.04$, $f_H = 1000$ MHz, $s = 1, 2, 3$;
- (b) x-mode, $A = 0.04$, $f_H = 1000$ MHz, $s = 1, 2, 3$;
- (c) o-mode, $A = 0.6$, $f_H = 600$ MHz, $s = 2, 3$;
- (d) x-mode, $A = 0.6$, $f_H = 600$ MHz, $s = 2, 3$;
- (e) o-mode and x-mode, $A = 1.0$, $f_H = 300$ MHz, $s = 1, 2$;
- (f) o-mode and x-mode, $A = 1.5$, $f_H = 300$ MHz, $s = 2$.

IV. RESONANCE ABSORPTION AT THE FIRST THREE HARMONIC LAYERS

Electromagnetic waves propagating in the equilibrium plasma where the electron density distribution is Maxwellian will be damped due to collision absorption and harmonic resonance absorption in the layers $\omega \approx s\omega_H$ ($s = 1, 2, 3$). It has been shown that in the solar corona only the harmonic resonance absorption needs to be considered (Ginzburg 1964). A most general and comprehensive theory on harmonic resonance absorption is given by Gershman (1960). According to Gershman,

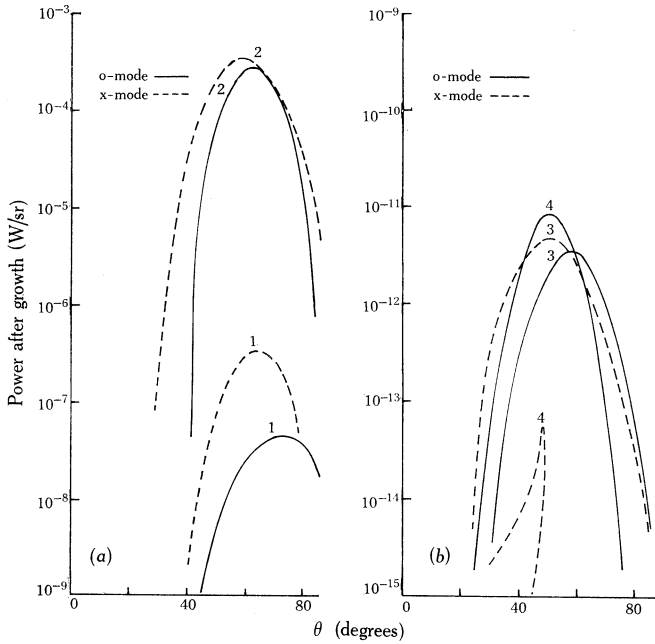


Fig. 6.—Power spectra after growth radiated by a single electron, with energy $E = 100$ keV and $\phi = 45^\circ$, for interaction time $t = 10^{-6}$ sec, $\sigma = 10^{-4}$, $s = 2$, and o-modes and x-modes for

- (a) curve 1: $A = 0.04, f_H = 1000$ MHz;
- curve 2: $A = 0.6, f_H = 600$ MHz;
- (b) curve 3: $A = 1.0, f_H = 300$ MHz;
- curve 4: $A = 1.5, f_H = 300$ MHz.

the electromagnetic wave propagating in the magnetoactive plasma is described by the form $\exp i\tilde{k}z$, where z is the path length in the direction of propagation (i.e. the wave vector direction) and $\tilde{k} = k + iq$, k being the wave number and q the absorption coefficient. The damping factor due to absorption becomes $\exp(-qz)$. Starting with the general dispersion equation, which is obtained by solving a linearized system of electromagnetic equations and kinetic equations for electrons, and investigating the absorption in the frequency region near $\omega \approx s\omega_H$, where $s = 1, 2, 3$, Gershman (1960) and Ginzburg (1964) obtained expressions for the first three harmonic specific resonance absorption coefficients as:

$$\left(\frac{q}{k}\right)_{s=1} = \left(\frac{2}{\pi}\right)^{\frac{1}{2}} \frac{\beta_T \cos \theta / X n_j}{2X - 2 - \sin^2 \theta + 2n_j^2 \sin^2 \theta} \left[\left\{ 1 - \left(1 - \frac{7}{4} \sin^2 \theta\right) X \right\} n_j^4 - \left\{ 2 + X \left(\frac{7}{4} \sin^2 \theta - \frac{5}{2} \right) + \frac{1}{4} X^2 (2 \cos 2\theta - \tan^2 \theta) \right\} n_j^2 + \left\{ 1 - \frac{3}{2} X + \frac{1}{2} X^2 (1 - \tan^2 \theta) + \frac{1}{4} X^3 \tan^2 \theta \right\} \right], \quad (8)$$

$$\left(\frac{q}{k}\right)_{s=2} = \left(\frac{\pi}{8}\right)^{\frac{1}{2}} \frac{X \beta_T n_j \sin^2 \theta}{\cos \theta} B(Y = \frac{1}{2}) \exp\left(\frac{-(1-2Y)^2}{2\beta_T^2 n_j^2 \cos^2 \theta}\right), \quad (9)$$

and

$$\left(\frac{q}{k}\right)_{s=3} = \frac{27}{8} \left(\frac{\pi}{8}\right)^{\frac{1}{2}} \frac{X \beta_T^3 n_j^3 \sin^4 \theta}{\cos \theta} B(Y = \frac{1}{3}) \exp\left(\frac{-(1-3Y)^2}{2\beta_T^2 n_j^2 \cos^2 \theta}\right), \quad (10)$$

where

$$B(Y) = \left(\frac{Y^2 - 1}{Y^2 n_j^2}\right) \left[\frac{1}{2} n_j^4 \sin^2 \theta + \left\{ X \left(\frac{1}{2} + \frac{1}{2} \cos^2 \theta + \frac{\sin^2 \theta}{1+Y} \right) - \left(1 + \frac{1}{2} \sin^2 \theta \right) \right\} n_j^2 + (1-X) \{ 1 - X/(1+Y) \} \right] \times \{ 2(1-Y^2 - X + Y^2 X \cos^2 \theta) n_j^2 - 2(1-X)^2 - (1 + \cos^2 \theta) Y^2 X + 2Y^2 \}^{-1}, \quad (11)$$

$\beta_T = (\kappa T / m_0 c)^{\frac{1}{2}}$ is the normalized thermal velocity of the electrons, κ is the Boltzmann constant, T is the temperature of the plasma in degrees Kelvin, $X = \omega_p^2 / \omega^2$, and $Y = \omega_H / \omega$. When $\omega \approx 2\omega_H$ we put $Y = \frac{1}{2}$ in (11) and when $\omega \approx 3\omega_H$ we use $Y = \frac{1}{3}$. In (9) and (10) the collision absorption term is omitted owing to the low collision frequency in the solar corona. For a plasma temperature in the solar corona of $T \sim 10^6$ K, the normalized thermal velocity $\beta_T \sim 10^{-2}$. Taking this into account, the harmonic specific resonance absorption for ordinary and extraordinary waves can be calculated and the s th harmonic resonance absorption coefficient q is found by multiplying the specific resonance absorption coefficient by k . Thus

$$q = (q/k)_s n_j \omega / c, \quad s = 1, 2, 3. \quad (12)$$

The curves in Figure 7 show the dependence of resonance absorption coefficients (q/f) on wave-normal angle θ for various values of X . The resonance absorption coefficient for extraordinary waves is always one to two orders of magnitude higher than the corresponding resonance absorption coefficient for ordinary waves. For all values of X , the resonance absorption is comparatively small when the wave-normal angle θ is less than 30° . The fourth harmonic resonance absorption layer, in general, is transparent to both extraordinary and ordinary waves (Zheleznyakov 1962). For the same harmonic number but higher wave frequency, resonance absorption takes place at a layer with higher magnetic field intensity and hence with greater resonance absorption. However, in this case, X becomes much smaller for higher frequencies if the electron density gradient is much less than the magnetic intensity gradient. As a result, the resonance absorption for the same harmonic number decreases with increasing frequency.

The power loss in passing through the resonance absorption layer is found by multiplying the value of the coefficient (q/f) given in Figure 7 by the thickness of the layer and the wave frequency (in MHz). The effective thickness of the absorption layer, according to Ginzburg and Zheleznyakov (1959), is

$$L = L_H \left(\frac{2}{3}\pi\right)^{\frac{1}{2}} n_j \beta_T \cos \theta, \tag{13}$$

where L_H is the characteristic length of the magnetic field of the sunspot in centimetres. Zheleznyakov (1962) defined the characteristic length of the magnetic field as

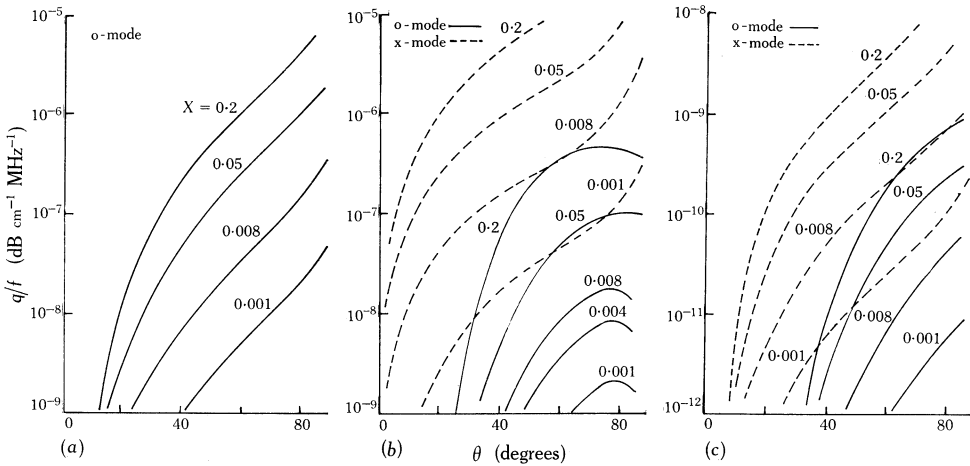


Fig. 7.—Variation of harmonic resonance absorption coefficient (q/f) for o-modes and x-modes with wave-normal angle θ for various values of X , $\beta_T = 10^{-2}$, and (a) $s = 1$, (b) $s = 2$, and (c) $s = 3$.

$L_H = H/\text{grad } H$. Therefore the effective thickness of the layer depends on the wave-normal angle θ and the characteristics of the sunspot magnetic field. For the lower active corona $\beta_T \sim 10^{-2}$ and $L_H = 10^9$ cm and the effective thickness of the absorption layer $L \sim 6 \times 10^6$ cm, if $\theta \sim 65^\circ$ and $n_j \sim 1$. Since the electron density gradient in the solar corona is much smaller than the magnetic field intensity gradient, the plasma frequencies in the first three resonance absorption layers for wave frequencies 6000–1000 MHz are similar. Thus, for simplicity, we take $f_p \sim 400$ MHz (see Fig. 1) and compute the power loss l_j (in decibels) for extraordinary and ordinary waves of frequencies 6000, 5000, 3500, 3000, 2000, and 1000 MHz on passing through the first three harmonic resonance absorption layers (Table 1). The first harmonic resonance absorption for extraordinary waves is not considered because extraordinary waves after passing through the layer $\omega \approx \omega_H$ cannot escape from the corona owing to the reflection at the layer $X = 1 - Y$. If I_{j0} and I_j are the powers of the j th normal wave before and after passing through the s th harmonic resonance absorption layer respectively, the fraction of power emerging from this layer is

$$R_j = I_j/I_{j0} = 10^{-l_j/10}, \tag{14}$$

where l_j is the power loss in decibels. Values of R_j are shown in Table 1. For all

cases, l_2 is less than l_1 and hence R_2 is greater than R_1 . We note that for frequencies 6000–1000 MHz in the lower solar corona the first and second harmonic resonance absorption layers are opaque to both extraordinary and ordinary waves. Although the third harmonic resonance absorption for extraordinary waves is larger than that for ordinary waves, for a sufficiently small value of X (i.e. for a sufficiently high frequency or a very low electron density) there is an appreciable fraction of extraordinary power emerging from the layer $\omega \approx 3\omega_H$, which is transparent to ordinary waves. As the X value increases gradually, the extraordinary power is cut off and only the ordinary wave carries significant power on leaving the layer $\omega \approx 3\omega_H$.

TABLE 1

POWER LOST AND TRANSMITTED BY O-WAVES AND X-WAVES OF VARIOUS FREQUENCIES ON PASSING THROUGH THE FIRST THREE HARMONIC RESONANCE ABSORPTION LAYERS

f (MHz)	s	X	Power Loss (dB)		R_j		S		P (%)	
			l_2	l_1	$j = 2$	$j = 1$	$r = 8$	$r = 5$	$r = 8$	$r = 5$
6000	1	0.0045	1.04(3)*	—	1(-104)	—				
	2		1.87(2)	8(3)	2(-19)	1(-800)				
	3		2.34(-1)	5.6	9.5(-1)	2.76(-1)	2.32	1.45	40	18.4
5000	1	0.0064	1.29(3)	—	1(-129)	—				
	2		2.55(2)	9.9(3)	3.12(-26)	1(-990)				
	3		2.85(-1)	6	9.36(-1)	2.5(-1)	2.13	1.34	36.2	14.5
3500	1	0.0079	1.1(3)	—	1(-110)	—				
	2		2.52(2)	8.5(3)	6.3(-26)	1(-850)				
	3		2.3(-1)	7.35	9.5(-1)	1.84(-1)	1.55	0.87	21.6	-7.0
3000	1	0.018	1.98(3)	—	1(-198)	—				
	2		4.15(2)	1.62(4)	3.16(-42)	1(-1620)				
	3		5.04(-1)	9.9	8.9(-1)	1.02(-1)	0.92	0.57	-4.15	-27.4
2000	1	0.04	3.12(3)	—	1(-312)	—				
	2		6(2)	2.64(4)	1(-60)	1(-2640)				
	3		7.8(-1)	1.56(1)	8.35(-1)	2.75(-2)	0.264	0.16	-58.1	-72.5
1000	1	0.16	6.6(3)	—	1(-660)	—				
	2		2.4(3)	6(4)	1(-240)	1(-6000)				
	3		1.5	2.52(1)	7(-1)	3(-3)	0.0344	0.022	-93	-95.5

* Each number in parentheses is the common logarithm of the multiplier; 1.04(3) means 1.04×10^3 .

V. ESCAPE OF CYCLOTRON RADIATION FROM THE LOWER SOLAR CORONA

After studying the characteristics of forward normal cyclotron radiation in both modes from electron streams and the propagation of electromagnetic waves in the solar corona we can predict the mode and degree of polarization of the emission observed on Earth.

For the forward normal cyclotron radiation, the normalized radiation frequency ξ is always greater than $\xi_0 = A^{\frac{1}{2}}$ or $\xi_x = \frac{1}{2}\{1 + (1 + 4A)^{\frac{1}{2}}\}$ and the source is above the reflection layers $X = 1$ or $X = 1 - Y$. Thus, if the electron stream gyrates outward from the Sun, the forward cyclotron radiation will be observed directly on Earth; on the other hand, forward radiation from electron streams travelling towards the Sun will only be observed after reflection. Assuming a spherically symmetrical electron density distribution (Fig. 1) for the solar atmosphere and neglecting the effect of the magnetic field, we find that the true escape level for

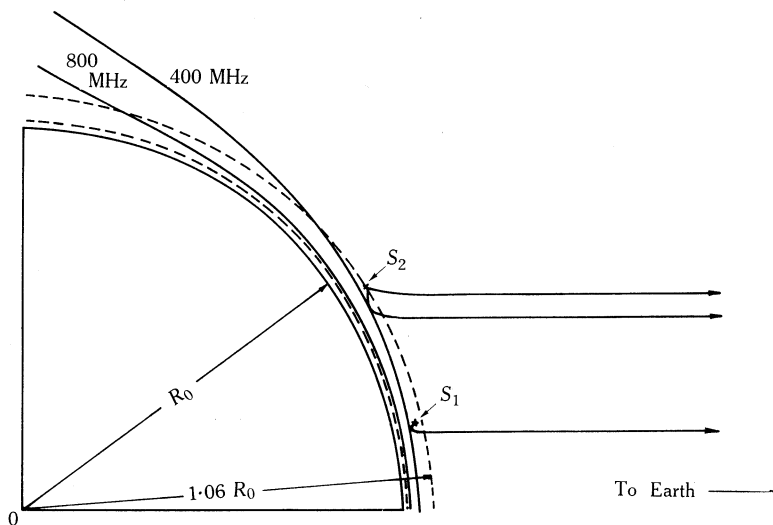


Fig. 8.—Escape levels in the active corona for waves of frequencies 400 and 800 MHz. The electron density distribution model given in Figure 1 is used. The layer between the dashed lines specifies the type IVA source region.

both modes of a particular frequency is higher than the plasma level $X = 1$ at the limb (Jaeger and Westfold 1950), and so radiation from a limb source may not be able to escape from the solar corona. This is demonstrated in Figure 8 for waves of frequencies 400 and 800 MHz. It can be seen that sources of lower frequency emissions will be more concentrated in the central area of the solar disk.

With electron energies of the order of 10–100 keV, maximum radiation after growth will be emitted with normalized frequency $\xi \gtrsim s$ and in a wave-normal angle $\theta_m \sim 50^\circ - 70^\circ$ if the electron pitch angle is not large. Thus the s th harmonic radiation will encounter only the $(s+n)$ th harmonic resonance absorption layers ($n = 1, 2, \dots$) in the neighbouring sunspot magnetic field. Since the field lines emerging from the sunspot area will be parallel to each other, the wave-normal angle θ at which the radiation passes through the resonance absorption layers will be close to θ_m . For very strong resonance absorption in the layer ($\omega \approx 2\omega_H$) the fundamental harmonic radiation in the ordinary mode (single-frequency solution) cannot be observed on Earth. The third harmonic radiation does not have to suffer strong harmonic resonance absorption owing to the transparency of the layer ($\omega \approx 4\omega_H$),

but, for $s = 3$, the rate of growth for both modes is much lower than that for the second harmonic radiation. From the discussion in Sections III(b) and III(c), the rates of growth and the emission powers for $s = 1$ and 2 are found to be of similar magnitude, but the former has to suffer much stronger resonance absorption at the layer $\omega \approx 2\omega_H$. Consequently, after passing through the layer $\omega \approx s\omega_H$ in the active corona, the second harmonic x-mode and o-mode waves carry most power, especially when the wave frequency is sufficiently high, and the third harmonic resonance absorption layer becomes completely transparent to o-mode waves and partly transparent to x-mode waves.

We now compare the second harmonic radiation power in x-mode and in o-mode escaping from the corona. As we have shown that the x-mode wave carries more power than the o-mode wave (see Fig. 6) and that when the value of X on the layer $\omega \approx 3\omega_H$ is small enough the resonance absorption is not very effective, the predominant power arriving on Earth is carried by the x-mode wave. Taking $f_p = 400$ MHz, $L_H \sim 10^9$ cm, $\beta_T \sim 10^{-2}$, $\theta \sim 65^\circ$, and $r = 5$, where r is the ratio of x-mode power to o-mode power before passing through the layer $\omega \approx 3\omega_H$ (Section III(c), point (4)), then the ratio S of x-mode power to o-mode power leaving this layer is greater than unity when the frequency f is greater than 3000 MHz. This is illustrated in Table 1. For emission at decimetre wavelengths ($f \lesssim 3000$ MHz), emitted from a source with larger A value, only the ordinary mode is observed on Earth, firstly because the rate of growth for o-mode exceeds that for x-mode as A increases (Section III(c), point (1)), and secondly because of the increase in X the effect of third harmonic resonance absorption becomes great enough to prevent the x-mode wave escaping from the corona. This explains why type IVA bursts are o-mode in decimetre wavelengths but x-mode in centimetre wavelengths (leading-spot hypothesis).

In general, cyclotron radiations in both modes from spiralling electron streams are elliptically polarized, but because of the propagation effect the high frequency radiation becomes circularly polarized except at $\theta \simeq 90^\circ$ in the boundary region (Piddington and Minnett 1951). For lower frequencies, the elliptically polarized radiation is gradually reduced to random and circularly polarized components owing to the Faraday rotation effect arising from propagation through the active region. According to Cohen (1958), the degree of polarization of the radiation in terms of circular components observed on Earth is defined as

$$P = \frac{I_1 - I_2}{I_1 + I_2} = \frac{S - 1}{S + 1}, \quad (15)$$

where I_1 and I_2 are the intensities of x-mode and o-mode waves escaping from the solar corona respectively and $S = I_1/I_2$. Following the hypothesis put forward by Weiss (1963), in the northern hemisphere left-handed polarization corresponds to emission in the ordinary mode if we assume that the sense of polarization is determined by the magnetic polarity of the leading spot. Thus the resultant radiation is left-handed polarized when P is negative and is right-handed polarized when P is positive. From (14) and (15), we have

$$S = r \times 10^{(l_s - l_o)/10}. \quad (16)$$

The sign of P changes at $S = 1$, that is, when the condition

$$\log_{10} r = \frac{1}{10}(l_1 - l_2) \quad (17)$$

is satisfied. For second harmonic forward emission, l_1 and l_2 are the power losses in decibels due to absorption at $\omega \approx 3\omega_H$ and $r < 10$. In other words, for a given value of r ($\gtrsim 1$) and under typical active corona conditions, there exists a frequency such that (17) holds. We call this frequency the transition frequency f_t . It has been shown in Section III that the greatest second harmonic radiation intensities in the x-mode and in the o-mode occur at similar wave-normal angles $\theta \sim 65^\circ$ for similar frequencies and that the radiation travels outward along nearly identical paths. Again taking $\theta \sim 65^\circ$, $\beta_T \sim 10^{-2}$, and $f_p \sim 400\text{--}450$ MHz, with the help of

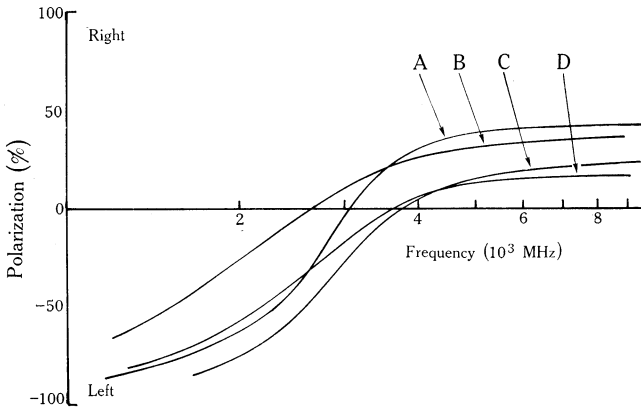


Fig. 9.—Variation of degree of polarization with wave frequency taking $\theta = 65^\circ$, $\beta_T = 10^{-2}$, and

- curve A: $f_p = 400$ MHz, $L_H = 10^9$ cm, $r = 8$;
- curve B: $f_p = 450$ MHz, $L_H = 5 \times 10^8$ cm, $r = 5$;
- curve C: $f_p = 400$ MHz, $L_H = 10^9$ cm, $r = 5$;
- curve D: $f_p = 450$ MHz, $L_H = 7.5 \times 10^8$ cm, $r = 5$.

Figure 7 and equation (15) the degree of polarization of the radiation can be calculated for various frequencies (Table 1). The dependence of degree of polarization on frequency is illustrated in Figure 9. Since the total radiation involves randomly polarized components arising from the Faraday rotation effect, eventually the observed degree of polarization is less than that given in Figure 9 and the values shown in Table 1 and Figure 9 are only approximate. Nevertheless, under certain active corona conditions, two points can be observed: (1) forward normal cyclotron radiation from electron streams changes the sense of polarization at some frequency between 2000 and 4000 MHz owing to the differential resonance absorption effect; (2) the degree of polarization is stronger in decimetre wavelengths than in centimetre wavelengths. These properties are completely in agreement with observation (Tanaka and Kakinuma 1959; Kundu 1965).

So far, we have considered the escape of harmonic cyclotron radiation of the single-frequency solution type. It has been shown by Fung and Yip (1966) that

whenever the source position satisfies the conditions (1) A close to unity, (2) near and above the level $f_H = f$, and (3) above the reflection level $X = 1$, an intense and narrow bandwidth burst radiation will be observed on Earth. In fact, when these conditions are met, the fundamental harmonic radiation in the ordinary mode is of the double-frequency solution type (Section III) and the corresponding power as well as the rate of growth sharply peak in a narrow frequency range and in a direction close to θ_c . If the electron energy is of the order of a few tens of keV, θ_c can be very small ($\lesssim 20^\circ$). Such emission will pass through the layer $\omega \approx 2\omega_H$ with small wave-normal angle θ and without significant power loss. Fundamental harmonic radiation in the extraordinary mode is emitted when A is small, but it cannot pass through the layer $\omega \approx 2\omega_H$ where strong resonance absorption for x-mode waves takes place even for small wave-normal angles (Fig. 7(b)).

VI. INTERPRETATION OF TYPE IVA BURSTS

The type IVA emission on centimetre and decimetre wavelengths is the first phase of the whole type IV event. It starts simultaneously with the explosive phase of a flare that is of importance 2 to 3+ and usually covers a large fraction of the umbral area of the sunspot group (Kundu 1965). During the occurrence of the flare phenomenon, electrons with energy up to 100 keV are ejected from the flare region in various directions in the form of electron streams (De Jager 1960). Those ejected in the forward direction radially will travel in the neutral plane or along the sunspot magnetic field line and will cause type III bursts by plasma wave radiation (Wild, Smerd, and Weiss 1963). Most of these electron streams are trapped in the neighbouring stronger sunspot magnetic field configuration forming helical electron streams with narrow momentum spread. They emit electromagnetic waves of different frequencies in both x-mode and o-mode by a cyclotron mechanism, giving rise to type IVA bursts (Fig. 10(a)). For certain large flares, such as those associated with type IV phenomena, fragments of plasma clouds with hydromagnetic shock wave fronts are expelled intermittently. Each plasma cloud with shock front ahead moves through the active solar corona with a speed ~ 1000 km/sec. Arriving at some region where the electron density is sufficiently low ($f_p \sim 100$ MHz), the shock front excites longitudinal oscillation, which in turn is converted into transverse electromagnetic radiation by Rayleigh scattering and combination scattering, and is finally observed as type II bursts (Fig. 10(b)). Therefore the type IVA emission occurs several minutes earlier than the type II bursts (Section I(x)).

The outermost field lines of the two bipolar pairs are highly disturbed by the plasma and merge together forming a single loop of a magnetic field line of force. Meanwhile, due to the high conductivity of the plasma cloud, this newly formed field line is frozen in and brought to a level as high as a few solar radii above the photosphere by the moving plasma cloud. Some more energetic electrons inside this cloud are accelerated to intermediate relativistic energies by a Fermi-like mechanism and gyrate along the frozen-in field line; radiation from these accelerated electrons is responsible for the type IVm emission (McLean 1959; Fung 1967) (Fig. 10(b)). At a later stage, this stretched field line remains in a steady position and eventually the type IVm emission may develop into a type I noise storm (Fung 1967).

As suggested by Fung (1967), the importance of a flare may be regarded as a rough measurement of the speed and quantity of plasma clouds ejected from the flare region. For a flare of lesser importance, the speed of the plasma cloud would be so low that no shock front would be formed or that the associated shock front would not be strong enough to excite a type II burst. Hence type IVA bursts associated with a less important flare could occur without type II and type IVm bursts. On the other hand, type IVm bursts would always associate with type IVA and type II bursts. This is consistent with observation.

Referring to the discussions in previous sections, type IVA bursts can be explained as follows.

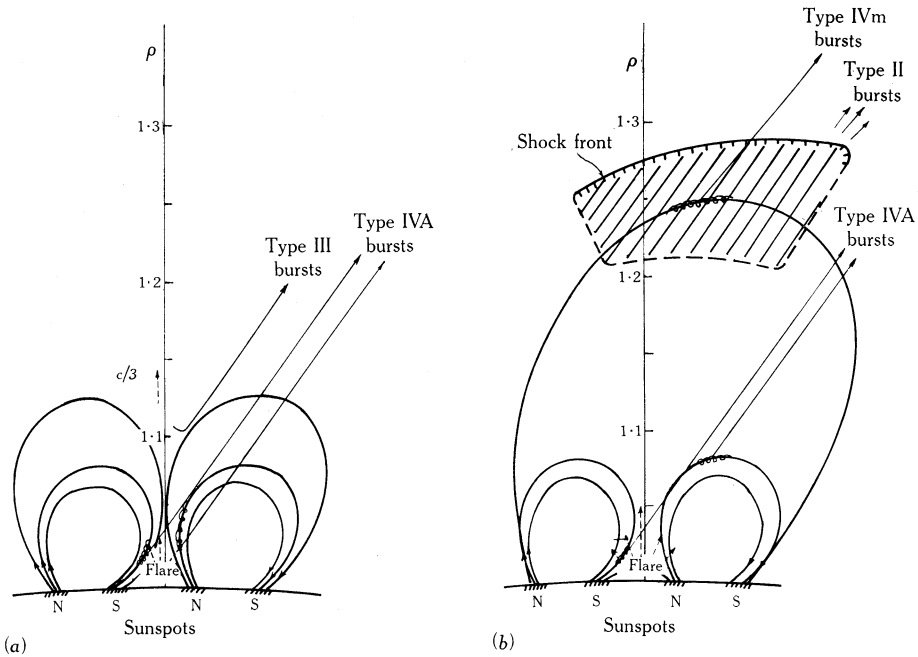


Fig. 10.—Schematic diagrams of the solar flare phenomenon and its associated radio emissions.

(a) Frequency Range and Frequency Drift

Assuming the model for the lower active corona as shown in Figure 1, the lowest emitting frequency for broad band second harmonic radiation can range from 10 000 to 500 MHz. The low frequency cutoff is either due to the limit of the intensity of the field line or to A being greater than four. For intense narrow bandwidth emission, A must be close to unity (shaded region in Fig. 1) and the corresponding gyrofrequency lies between 1000 and 400 MHz. Therefore the variabilities occur in the decimetre wavelength region.

Because of the large gradients of electron density distribution and sunspot magnetic intensity in the transition region (the region between the corona and the chromosphere), for electron energy $E \sim 100$ keV the fundamental harmonic emission frequency can drift through a frequency range of the order of 200–400 MHz within 1 sec. The extremely slow drift occurring in a few decimetre wavelength continuum bursts is probably due to the decrease of magnetic field intensity of the source (Takakura 1963). This is supported by the optical observation that a decrease in the magnetic field gradient and sometimes in the magnetic field energy occurs during a flare (Severnyi 1966).

(b) *Duration and Bandwidth*

Whenever the single-frequency solution condition is satisfied for the generating process, the second harmonic emissions in both modes have a broad bandwidth and cone of emission. Many such broad band emissions from the low level of the active corona will superimpose upon each other to form a long-lived broad band continuum in centimetre and decimetre wavelength regions. For the same electron energy, electron pitch angle, and A value, the actual half-power bandwidth is proportional to the local gyrofrequency and the centimetre wavelength bursts have broader bandwidth, while the narrow bandwidth fundamental harmonic o-mode emissions in decimetre wavelengths are grouped together and superimposed on the background continuum, appearing as the fine structure or patchiness in the dynamic spectrum.

The electron streams trapped in the sunspot magnetic field configuration can remain there for a certain time, but, as pointed out by Fung (1966c), the narrow momentum spread and hence the possibility of growth of power cannot last for a period as long as 1 hr, owing to diffusion and curvature drift. Thus the long duration of type IVA bursts should be attributed to the continuous expulsion of energetic electrons from the flare region. The longer duration observed in the decimetre wavelength region may be the result of high frequency extensions of type IVm emission (Smerd 1964).

(c) *Polarization*

The change of modes of polarization of type IVA bursts is due to differential harmonic resonance absorption. This has been discussed in detail in Sections IV and V. It should be mentioned that the transition frequency depends on the lower corona conditions, i.e. electron density and magnetic intensity gradient.

(d) *Angular Size and Directivity*

Michard (1963) indicated that the probability of a flare with type IV bursts or a polar blackout increases as the distance between spots decreases. Also the type IVA bursts are emitted at a low altitude in the corona. Hence the diameter of a type IVA emission source is smaller than that of a type I noise storm source. The slight directivity of the decimetre wavelength bursts towards the centre of the solar disk has been mentioned in Section V.

VII. CONCLUSIONS

Adopting the current model for solar flare evolution, type IVA emission is well accounted for by the Doppler-shifted cyclotron radiation theory. In spite of their distinct source characteristics, type IVA and type IVm bursts can result from the explosion of the same large flare above a complex sunspot group during the late phase of the solar cycle. They are similar in appearance on the dynamic spectrum. In order that a type IV event can be satisfactorily interpreted, we have to consider the active corona condition and the propagation of electromagnetic waves in the solar corona as well as the electron-trapping pattern. Radio and optical observations during previous solar cycles lead to the conclusion that there are two phases of fast electrons created during a flare period (Wild, Smerd, and Weiss 1963): (1) a succession of bursts of electrons (~ 100 keV) produced by conversion of magnetic energy into kinetic energy owing to plasma instability in the magnetic neutral region, and (2) thermal electrons accelerated to higher energies by the magnetohydrodynamic shock wave front through a Fermi process. The second phase is initiated by the first and occurs only in large flares associated with type IV phenomena. During the occurrence of a very large flare, the electrons of the first phase released from the flare region cause type III, V,* and IVA burst emissions; while those of the second phase arising from the ejection of a plasma cloud radiate type IVm bursts, and the associated magnetohydrodynamic shock wave front excites type II emission. All these nonthermal radio emissions are associated with the same large flare and appear consecutively. The type I noise storms, also regarded as the consequence of cyclotron radiation from electron streams, often occur alone after the start of a flare of less importance and are usually not preceded by a type IV emission. This indicates that radiation electrons responsible for type I radio emission would be produced and trapped in the sunspot magnetic field in different ways or in different regions. Moreover, the sunspot magnetic field configuration and intensity gradient will change after the flare (Severnyi 1966) and it is to be expected that type IVA and type I emissions will possess some different spectral properties.

VIII. ACKNOWLEDGMENT

The author wishes to express his thanks to Professor G. R. A. Ellis, Physics Department, University of Tasmania, for his critical reading of the manuscript and valuable suggestions.

IX. REFERENCES

- ALLEN, C. W. (1947).—*Mon. Not. R. astr. Soc.* **107**, 426.
 BOISCHOT, A. (1957).—*C. r. hebd. Séanc. Acad. Sci., Paris* **244**, 1326.
 BOISCHOT, A., and DENISSE, J. F. (1957).—*C. r. hebd. Séanc. Acad. Sci., Paris* **245**, 2199.
 COHEN, M. H. (1958).—*Proc. Inst. Radio Engrs* **46**, 172.
 DE JAGER, C. (1960).—“Space Research.” (Ed. H. Kallmann-Bijl.) Vol. 1, p. 628. (North Holland: Amsterdam.)
 DENISSE, J. F. (1960).—*Inform. Bull. S.R.O.E.* No. 4, p. 3.

* At present, theory on the origin of type V emission is not well established although a suggestion has already been put forward by Weiss (1965).

- ELLIS, G. R. A. (1964).—*Aust. J. Phys.* **17**, 63.
- FUNG, P. C. W. (1966a).—*Planet. Space Sci.* **14**, 469.
- FUNG, P. C. W. (1966b).—*Planet. Space Sci.* **14**, 335.
- FUNG, P. C. W. (1966c).—Ph.D. Thesis, University of Tasmania.
- FUNG, P. C. W. (1967).—The origin of solar type IV metre-wave storms. (To be published.)
- FUNG, P. C. W., and YIP, W. K. (1966).—*Aust. J. Phys.* **19**, 759.
- GERSHMAN, B. N. (1960).—*Soviet Phys. JETP* **11**, 657.
- GINZBURG, V. L. (1964).—“The Propagation of Electromagnetic Waves in Plasma.” (Pergamon Press: New York.)
- GINZBURG, V. L., and ZHELEZNYAKOV, V. V. (1959).—*Soviet Astr. AJ* **3**, 235.
- HADDOCK, F. T. (1959).—Symp. IAU No. 9 (Paris 1958). p. 188.
- IVANOV-KHOLODNYI, G. S., and NIKOL'SKII, G. M. (1962).—*Soviet Astr. AJ* **6**, 609.
- JAEGER, J. C., and WESTFOLD, K. C. (1950).—*Aust. J. scient. Res. A* **3**, 376.
- KUNDU, M. R. (1959).—*Annls Astrophys.* **22**, 1.
- KUNDU, M. R. (1961).—*Astrophys. J.* **134**, 96.
- KUNDU, M. R. (1965).—“Solar Radio Astronomy.” (Wiley: New York.)
- KUNDU, M. R., and FIROR, J. W. (1961).—*Astrophys. J.* **134**, 389.
- KUNDU, M. R., ROBERTS, J. A., SPENCER, C. L., and KUIPER, J. W. (1961).—*Astrophys. J.* **133**, 255.
- KUNDU, M. R., and SPENCER, C. L. (1963).—*Astrophys. J.* **137**, 572.
- LIEMOHN, H. B. (1965).—*Radio Sci.* **69D**, 741.
- MCLEAN, D. J. (1959).—*Aust. J. Phys.* **12**, 404.
- MICHARD, R. (1963).—Symp. IAU No. 22 (Rottach-Eggern 1963). p. 373.
- MORIMOTO, M., and KAI, K. (1961).—*Publs astr. Soc. Japan* **13**, 294.
- NEWKIRK, G. (1959).—Symp. IAU No. 9 (Paris 1958). p. 149.
- PICK, M. (1961).—*Annls Astrophys.* **24**, 183.
- PIDDINGTON, J. H., and MINNETT, H. C. (1951).—*Aust. J. scient. Res. A* **4**, 131.
- SEVERNYI, A. B. (1966).—*Soviet Phys. Usp.* **9**, 1.
- SHAIN, C. A., and HIGGINS, C. S. (1959).—*Aust. J. Phys.* **12**, 357.
- SMERD, S. F. (1964).—“Research in Geophysics.” (Ed. H. Odishaw.) Vol. 1, p. 89. (M.I.T. Press.)
- TAKAKURA, T. (1960a).—*Publs astr. Soc. Japan* **12**, 55.
- TAKAKURA, T. (1960b).—*Publs astr. Soc. Japan* **12**, 325.
- TAKAKURA, T. (1960c).—*Publs astr. Soc. Japan* **12**, 352.
- TAKAKURA, T. (1962).—*J. phys. Soc. Japan*, Suppl. A-II **17**, 243.
- TAKAKURA, T. (1963).—*Publs astr. Soc. Japan* **15**, 327.
- TAKAKURA, T., and KAI, K. (1961).—*Publs astr. Soc. Japan* **13**, 94.
- TANAKA, H., and KAKINUMA, T. (1959).—Symp. IAU No. 9 (Paris 1958). p. 215.
- THOMPSON, A. R., and MAXWELL, A. (1962).—*Astrophys. J.* **136**, 546.
- WEISS, A. A. (1963).—*Aust. J. Phys.* **16**, 526.
- WEISS, A. A. (1965).—*Aust. J. Phys.* **18**, 143.
- WILD, J. P., SMERD, S. F., and WEISS, A. A. (1963).—*Ann. Rev. Astr. Astrophys.* **1**, 291.
- YOUNG, C. W., SPENCER, C. L., MORETON, G. E., and ROBERTS, J. A. (1961).—*Astrophys. J.* **133**, 243.
- ZHELEZNYAKOV, V. V. (1962).—*Soviet Astr. AJ* **6**, 3.

